THE ASTROPHYSICAL JOURNAL, 439:860–874, 1995 February 1

CLASSICAL ROTATIONAL BROADENING OF SPECTRAL LINES

GEORGE W. COLLINS II
Warner and Swasey Observatory, Case Western Reserve University, Cleveland, OH 44106
AND
RYLAND J. TRUAX
Ohio State University, 174 West 18th Avenue, Columbus, OH 43210
Received 1994 April 18; accepted 1994 August 5

ABSTRACT

In this paper we investigate the extent to which the classical approach to stellar rotation can yield reliable estimates of the projected stellar rotational velocity. We compare the classical picture of stellar rotation developed by Carroll, Struve, Unsöld, and others with ab initio models of rotating stellar atmospheres having known characteristics. We estimate the extent to which the differences between the simple model and the more physically motivated model can be attributed to various assumptions of the simple model. In addition to the simplest model envisioned by early investigators, we consider the use of an empirically determined "sharp-line profile" in conjunction with the classical model, and the extent to which this improves the results. Particular attention is paid to the effects of limb darkening both in the line and in the continuum.

To accomplish this comparison between these two classes of models, we employ two traditional methods of analysis for rotationally broadened line profiles, the relation of the half-width of the line, and the zeros of the Fourier transform of the line as measures of the projected rotational velocity of the star. This analysis is carried out both for the early assumption that the local stellar line profile can be represented by a strong, arbitrarily sharp line and for the more common case where the local line profile can be approximated by a flux profile appropriate for a similar star that shows no rotation.

We find that stars exhibiting rapid rotation are poorly described by the classical model in any form. What is somewhat surprising is that even early-type stars showing moderate rotation may suffer significant departures from the classical model. Inappropriate treatment of the limb darkening seems to be a central reason for the breakdown of the classical model at modest speeds. Applications of the classical model as a probe of the more sophisticated aspects of the atmospheric velocity field, such as differential rotation, zonal wind flow, and turbulence, are discussed. As expected because of the departure of the projected rotational speed of the classical model from that of more complete models, the use of the classical treatment for more subtle aspects of the stellar velocity field is problematic at best.

Subject headings: line: profiles — stars: atmospheres — stars: rotation

1. INTRODUCTION

The realization that large-scale rotation can affect the shape of spectral lines can be traced back nearly as far as the discovery of stellar spectra itself. However, it was not until the paper by Shapley & Nicholsen (1919) that there was any attempt to formalize the concept of rotational broadening of spectral lines. Any attempt to discover the nature of the photospheric velocity field from the analysis of spectral lines requires the modeling of that velocity field as well as the atmospheric structure that gives rise to the observed spectral lines. The early models of stellar rotation assumed that the only velocity affecting the spectral lines arose from a uniform macroscopic rotation of the entire star itself seen at some angle of inclination.

In this paper we investigate the extent to which this classical model of rotating stars developed by Carroll (1928) and Shajn & Struve (1929), and its subsequent modification by many others, can be used to provide quantitative information about the atmospheric velocity field displayed to an observer. We shall confine our attention to the early-type stars, since their large rotational velocities can be expected to provide the most severe tests for any model. The classical model of rotating stars and its subsequent modification are filled with explicit and implicit assumptions affecting the applicability of the model to the analysis of actual stars. We will investigate the effect of some of these assumptions on the determination of stellar rotational velocities by applying the analytical techniques suggested by the classical model to spectral lines resulting from a model based on the best rotating model stellar atmospheres currently available. This approach has the advantage that we know the stellar parameters that produced the rotationally broadened spectral lines with the precision of initial values, and the "observational error" can be limited to the numerical accuracy to which the calculations can be made. By investigating the application of the classical model to the analysis of the spectral lines of this ab initio model, we hope to establish the extent to which the classical model can be used to describe the global rotation of the star. This will allow us to determine the extent to which differences between the classical model and observation can be interpreted as resulting from other aspects of the atmospheric velocity field (e.g., differential rotation, zonal wind flows, and turbulence).

The classical model of a rotating star can be viewed as presenting a circular disk darkened by classical linear limb darkening to the observer. The earliest form of this model assumes that the spectral line formed locally on the surface of the star is arbitrarily sharp but has a finite equivalent width. We shall refer to this model as the classical model of a rotating star

(CMRS). Later, this assumption was replaced by the notion that the local spectral line could be empirically represented by one obtained from the observation of a "sharp-lined star" of the same spectral type. We shall refer to this modification of the classical model of a rotating star by the acronym MCMRS.

The CMRS was developed from somewhat different points of view by Carroll (1928) and Shajn & Struve (1929), and later expanded by Unsöld (1955). In this version the arbitrarily sharp spectral line is rotationally broadened in a star showing no photospheric structural variation over its spherically symmetric surface. This early form of the CMRS has the obvious benefit of excluding any of the detailed physics required to describe the formation and structure of actual atomic line profiles. It has the associated disadvantage that it cannot possibly describe accurately the profiles of real lines. The early attempts to include aspect effects of viewing the photosphere through the inclusion of a linear limb-darkening law were refined by Unsöld, and we shall discuss the effects of introducing this modification. However, the very lack of the details of line formation allows us to separate the effects of the geometry of the macroscopic rotation and the effects of limb darkening of the photospheric continuum from the more complicated effects of line formation. Thus, we shall begin our investigation in § 2 by delineating the assumptions of the CMRS and presenting line profiles and their Fourier transforms which result from this most basic model.

However, most of the determination of stellar rotational velocities involves the MCMRS, where the assumption of the "delta-function–like" line profile of the early model is replaced by the profile of a "sharp-lined star" which is subsequently rotationally broadened in the classical manner. This clearly has the advantage of eliminating the ad hoc aspects of the classical line and sidesteps the problems of line formation by using an empirical line. Unfortunately, the use of empirical lines, of necessity, includes uncertainties as to the applicability of the stellar conditions giving rise to the line and their compatibility with the target of the investigation. By utilizing a nonrotating model having the same mass, radius, and luminosity as the rotating models, we can simulate analysis using this modified form of the classical model that we have denoted by MCMRS. After describing the nature of the ab initio models in § 3 and comparing them with the results of the CMRS, we shall determine the value of the limb-darkening coefficient appropriate for the continuum from the ab initio models. Section 4 will analyze the ability of the MCMRS to yield accurate values for the macroscopic rotational equatorial velocity projected along the line of sight (i.e., $V_e \sin i$). Particular attention is paid to the differences between the limb darkening of the continuum and that appropriate for the rotationally broadened line. Having ascertained the efficacy of the CMRS and MCMRS to determine the zero-order aspect of rotational broadening, we shall look into the prospects of using departures from the classical models to determine other aspects of the photospheric velocity field in § 5. We shall conclude by summarizing the impact of these results on the existing literature and their implications for future work.

There are two traditional approaches to the analysis of spectral lines: the investigation of the observed line profiles themselves, and the analysis of the Fourier transforms of those lines. Each has its good and bad points. We shall consider both approaches for both the CMRS and the MCMRS, so that a quantitative comparison can be made between them. While it would be possible to make comparisons between the classical model and more physically motivated models for a wide range of stars on the H-R diagram, we will concentrate on main-sequence B stars, since they exhibit the widest range of rotational velocities among the normal stars. Finally, in order to make the distinction clear between rotational velocities obtained by measuring properties of the line profile and the actual values of the rotational velocities, we shall donate the former by $V \sin i$ and the latter by $V_e \sin i$. As we shall see, values of $V \sin i$ obtained from line profiles may have little to do with the value of the equatorial velocity multiplied by the sine of the inclination (i.e., $V_e \sin i$).

2. THE CLASSICAL MODEL OF ROTATIONAL LINE BROADENING

Early discussions of rotational broadening of spectral lines were initiated by Shapley & Nicholsen (1919) but were not developed until the work of Carroll (1928, 1933) and Shajn & Struve (1929). While Carroll & Ingram (1933) applied the theoretical development to actual stellar systems, it is Struve's name that is most strongly associated with stellar rotation, because of his pursuit of the study over the following quarter-century. In addition, the graphical presentation of the basic theory of stellar rotation given by Shajn & Struve (1929) is more approachable and, at that time was computationally more accessible than the more esoteric development of Carroll (1928, 1933). As indicated above, Carroll (1933) correctly recognized the importance of limb darkening to the problem and formulated the approach for its inclusion, but it remained for Unsöld (1955) to provide a clear extension of Carroll's (1933) development to arbitrary limb darkening. Even here, the limb darkening remained a "*combined law of darkening.*" Since this form for the description of a rotating star has supplied the basis for understanding stellar rotation for most of the century, we shall refer to it as the classical model of a rotating star.

Although Shajn & Struve's (1929) graphical description of a rotating star was for a uniformly bright star, Carroll (1928) had introduced limb darkening to the model in 1933, and it remains a central part of the model. However, as described by Gray (1976), the limb darkening is taken to be that appropriate for the continuum adjacent to the line. This leads to the following assumptions on which the model is based:

1. The observational aspect of a uniformly rotating star may be approximated by a circular disk subject to a linear limb-darkening law applicable to all parts of the stellar disk (see eq. [1]).
2. The limb-darkening law and coefficient appropriate for the radiation in the line are the same as for the continuum.
3. The form of the line does not change over the apparent disk; it is simply uniformly Doppler-shifted by the radial motion resulting from the rotation.

The first of these assumptions results in the radial velocity and hence the Doppler shift of the line being constant along chords parallel to the meridian plane of the star. This is the core of the Shajn & Struve (1929) graphical representation (see Fig. 1*a*). The contribution to the convolved profile arising from any chord will simply be the local profile Doppler-shifted by the proper amount and weighted by the length of the chord adjusted for limb darkening. The limb-darkening law can simply be represented by

$$I(\mu) = I_0[1 - \alpha(1 - \mu)] = I_0(1 + \beta\mu)/(1 + \beta)\,, \qquad (1)$$

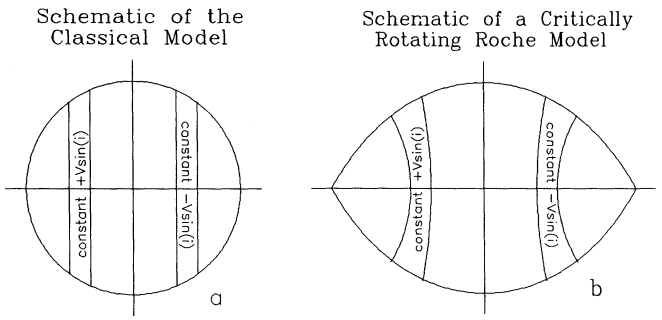

FIG. 1.—Schematic representation of the apparent disk of a rotating star as represented by (*a*) the CMRS and (*b*) a uniformly critically rotating Roche model seen equator-on. Note that the lines of constant $V_e \sin i$ no longer lie on chords as they do in the CMRS.

where I_0 is the specific intensity at the center of the disk. Here the second form involving β is that given by Unsöld (1955), and we present it for comparison. The relation between the usual limb-darkening coefficient α as described by Gray (1976) and β as used by Unsöld (1955) is

$$\beta = \alpha/(1 - \alpha) . \tag{2}$$

While this assumption would seem approximately correct for the modest values of rotation originally anticipated by Carroll (1933), it fails measurably for the large rotational velocities that characterize many stars on the upper main sequence, particularly the Be stars. Here the distortion of the apparent stellar disk may reach 50% for critically rotating stars viewed equator-on (see Fig. 1*b*). In addition, the presence of gravity darkening as initially described by von Zeipel (1924) will further destroy the axial symmetry about the line of sight that leads to the simple geometrical representation of Shajn & Struve (1929).

The impact of the second assumption on the CMRS is quite subtle. Even though the nature of the line is arbitrarily sharp, it is assumed to have a finite equivalent width. Such a line can be subject to limb darkening by reducing the local contribution to the equivalent width in accordance with the reduction of the continuum intensity resulting from limb darkening. That reduction can be made in accordance with assumption 2 and is in much of the development of the MCMRS as well as the CMRS. Unlike the first assumption, the second and third fail for even modest values of rotation. A perusal of the simple Milne-Eddington atmosphere model for spectral lines (e.g., Collins 1989) shows that the strength and shape of an absorption line will depend on several factors, such as the local temperature gradient and the relative strength of the line absorption coefficient relative to the total absorption (that is, η_ν). Since neither of these factors is present in the CMRS, we can conclude that the CMRS is, at best, incomplete. The variation of the ionization-excitation equilibrium over the surface of a rapidly rotating star, together with the presence of shape distortion and gravity darkening mentioned above, will further violate these last two assumptions.

Before investigating the extent to which these assumptions bear on the shape of rotationally broadened lines and their Fourier transforms, it is worth briefly reviewing the influence of limb darkening. Gray (1976) uses assumption 3 to justify assumption 2, so the value of the limb-darkening coefficient to be used is unambiguously that of the adjacent continuum. We may test the extent to which this is justified by considering the Milne-Eddington model for a stellar atmosphere where the source function in the continuum and line is the Planck function, given by the linear relations

$$B_c(\tau_c) = a + b\tau_c ,$$
$$B_\nu(\tau_\nu) = a + b\tau_\nu = a + b\tau_c/(1 + \eta_\nu) , \tag{3}$$

where η_ν is a measure of the relative strength of the line extinction coefficient and is given by

$$\eta_\nu = (\kappa_\nu + \sigma_\nu)/\kappa_c . \tag{4}$$

The Milne-Eddington model assumes η_ν is independent of depth in the atmosphere. Since the emergent intensity is the Laplace transform of the optical depth dependence of the source function, it is immediately possible to relate the parameters a and b describing the linear behavior of the source function to the value of the linear limb-darkening coefficient α given by equation (1). If we compare the value of α in the continuum to that appropriate for the line, we get

$$\alpha_c/\alpha_\nu = 1 + a\eta_\nu/(a + b) . \tag{5}$$

Thus, when the spectral line in question is weak (i.e., $\eta_\nu \ll 1$) or the source function gradient in the continuum is large (i.e., $b/a \gg 1$), assumption 2 should be justified. This would be the case for weak optical lines in the late-type stars. However, for the rapidly rotating stars of the upper main sequence, rotation broadens the lines to such an extent that only the strongest lines are visible in the spectrum. In addition, in the optical part of the spectrum, the lines lie on the Rayleigh-Jeans tail of the spectral energy distribution, leading to a rather small value of the source function gradient, hence a small value of b/a. Thus, we should expect that assumption 2 fails for these stars, and its adoption for their analysis may lead to erroneous values for their rotational velocity.

Even for those stars for which assumption 2 is valid, the value of the limb-darkening coefficient will depend sensitively on the spectral type and the wavelength region involved. Indeed, when $b \gg 1$, the limb-darkening coefficient will also be large. Thus, we should see to what extent the limb darkening affects a rotationally broadened line. While Carroll (1933) considered limb darkening for $\alpha = 0.6$, a more general discussion remained for Unsöld's (1955) treatment. He clearly shows that rotational line broadening of an undarkened star will yield an elliptical profile (see Fig. 2*a*). As the limb darkening becomes progressively stronger, the resulting reduced contribution of the most rapidly rotating regions of the star deforms the profile to a limiting parabolic shape (i.e., the dashed line of Fig. 2*a*). In addition to affecting the half-widths of the rotationally broadened lines (see eqs. [9]–[11] below), this change will shift the zeros of the Fourier transform of the line profiles associated with the CMRS to larger values (see Fig. 3). Using slightly different notation, Gray (1988) shows this effect for intermediate values of the limb-darkening coefficient. Since the shift from an elliptical to a parabolic profile is a global change in the line profile, the largest changes to the zeros of the Fourier transform will be found in the smallest values associated with the lowest frequencies. This can be seen by finding the zeros of the Fourier transform of the broadening function $\tilde{g}(v)$ of the CMRS given by Unsöld (1955, p. 513), which is

$$\tilde{g}(v) = \frac{6(1 - \alpha)}{3 - \alpha} \left\{ \frac{J_1(v\xi)}{v\xi} - \frac{\alpha}{1 - \alpha} \left[\frac{\cos(v\xi)}{(v\xi)^2} - \frac{\sin(v\xi)}{(v\xi)^3} \right] \right\} . \tag{6}$$

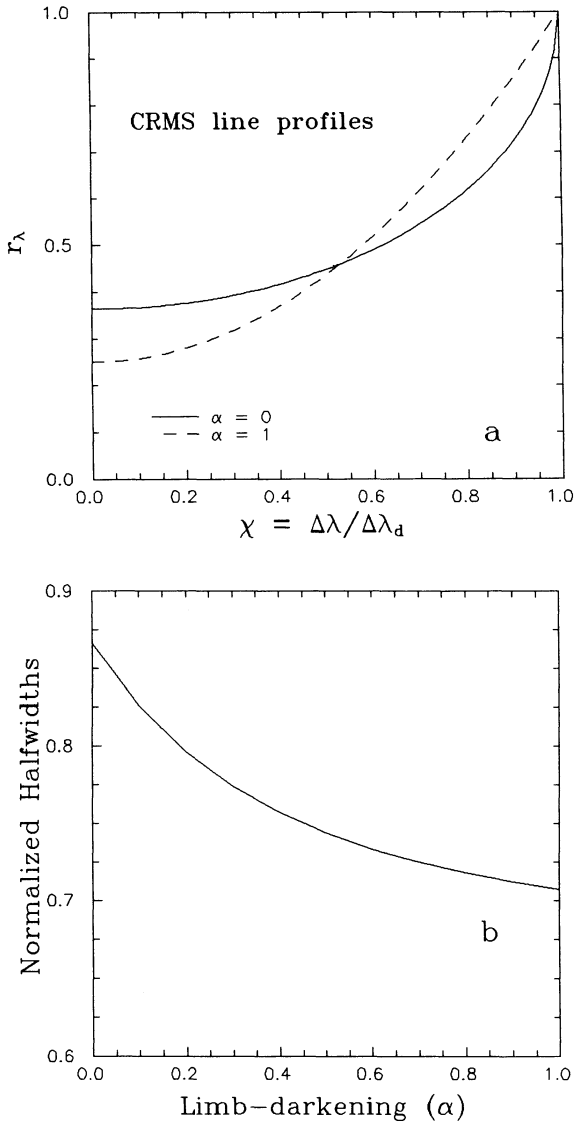

FIG. 2.—(*a*) Variations of the classical rotationally broadened line profile for the extreme values of limb darkening. A uniformly bright disk produces the elliptical profile and has a value of $\alpha = 0$. A fully darkened star yields a parabolic profile and $\alpha = 1$. (*b*) Range of half-widths associated with the variation of α. The measured half-width here has been normalized by the Doppler width as discussed in the text.

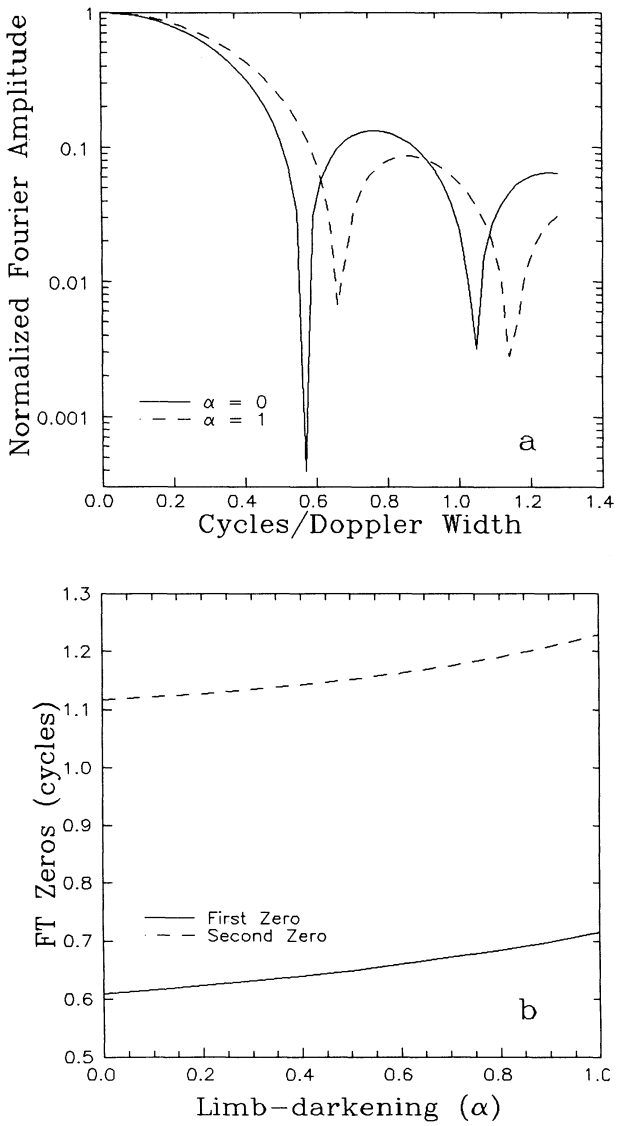

FIG. 3.—(*a*) Same as Fig. 2, but for the Fourier transforms of the line profiles given in Fig. 2*a*. (*b*) Variation of the first two zeros of the Fourier transform with limb darkening.

The values for the first five zeros, $x_i = (\xi\nu)_i/2\pi$, of this function are given in Table 1. The units chosen are cycles rather than radians, for the purpose of compatibility with earlier work. This work is extended by giving results for a full range of values of the limb-darkening coefficient α. The range of the first zero for all possible values of the limb darkening is about 16% around Carroll's value for $x_1(\alpha = 0.6)$, while the corresponding range of $x_4(\alpha)$ associated with the higher frequency behavior of the line profile is reduced to 4.5%. The parameter ξ is related to the rotational velocity by

$$\xi = \lambda_0\left(\frac{V \sin i}{c}\right). \tag{7}$$

The Fourier transform $F(f)$, of the observational profiles will have units that are the inverse of the profile itself, but it will have zeros in f that are related to the zeros of the Fourier transform of the broadening function $\tilde{g}(v)$ so that

$$f_i \xi = x_i\,. \tag{8}$$

Thus variations in x_i are reflected in variations in ξ and hence in V sin i. However, it is the spacing between the zeros of $F(f)$ that is taken as the hallmark of rotation, for it is characteristic of the global shape of the rotationally broadened profile and is mirrored in the zeros of the CMRS. Unfortunately, observational values of the higher order zeros are affected by the presence of noise in the original line profile as well as the sampling frequency within the original line. Thus, practice tends to limit analysis to the lower order zeros so affected by limb darkening and other phenomena which subtly change the overall line shape.

The zeros of the Fourier transform of the line profile convey information about the value of V sin i associated with the rotationally broadened line. A single characteristic of the line

TABLE 1

ZEROS OF FOURIER TRANSFORMS OF CMRS BROADENING FUNCTION

α	x_0	x_1	x_2	x_3	x_4	β
0.0	0.60984	1.11656	1.61916	2.12053	2.62138	0.000
0.1	0.61636	1.12179	1.62364	2.12451	2.62501	0.111
0.2	0.62349	1.12773	1.62882	2.19191	2.62929	0.250
0.3	0.63132	1.13455	1.63492	2.13473	2.63441	0.429
0.4	0.63995	1.14243	1.64211	2.14138	2.64064	0.666
0.5	0.64947	1.15160	1.65074	2.14951	2.64832	1.000
0.6	0.66001	1.16236	1.66121	2.15961	2.65805	1.500
0.7	0.67171	1.17508	1.67409	2.17237	2.67060	2.333
0.8	0.68471	1.19019	1.69011	2.18883	2.68725	4.000
0.9	0.69915	1.20817	1.71023	2.21038	2.70982	9.000
0.999.....	0.71498	1.22928	1.73515	2.23839	2.74041	999.000

NOTE.—Values of x_i are in units of cycles.

TABLE 2

NORMALIZED HALF-WIDTHS $\chi_{1/2}$ FOR REPRESENTATIVE LIMB-DARKENING VALUES

α	$\chi_{1/2}$	β
0.0.....	0.86603	0.000
0.1.....	0.82602	0.111
0.2.....	0.79614	0.250
0.3.....	0.77394	0.429
0.4.....	0.75710	0.666
0.5.....	0.74400	1.000
0.6.....	0.73356	1.500
0.7.....	0.72508	2.333
0.8.....	0.71805	4.000
0.9.....	0.71214	9.000
1.0.....	0.70711	∞

profile itself that contains the same information is the full width of the line at half-maximum depth (FWHM). In the CMRS the line profile of an intrinsically sharp line (i.e., one given locally by a delta function) ranges from ellipsoidal to parabolic depending on the value of the limb-darkening coefficient. Thus, just as the zeros of the Fourier transform of the line profile depend on the limb darkening, so the FWHM of the line will also depend on the value of the limb-darkening coefficient. Following the development of Unsöld (1955), Collins & Cranmer (1991) give the flux in such a rotationally broadened line as

$$F(\chi) = \frac{\pi J}{2}\left\{1 - \frac{1}{1+2\beta/3}\left[\frac{2}{\pi}(1-\chi^2)^{1/2} + \frac{\beta}{2}(1-\chi^2)\right]\right\}, \quad (9)$$

where χ is the dimensionless frequency shift,

$$\chi \equiv \Delta\lambda/\Delta\lambda_D = \Delta\lambda/\xi\,. \quad (10)$$

From equation (9) one can then calculate the value of $\chi_{1/2}$ for which the value of the flux drops halfway toward its minimum value at $\chi = 0$ and get

$$\chi_{1/2} = \frac{1}{2} + \frac{[(1+\beta\pi)^2 + \beta^2\pi^2]^{1/2} - (1+\beta\pi)}{2\beta^2\pi^2}$$

$$= \frac{1}{2} + \frac{1-\alpha}{2\alpha^2\pi^2} \times [\{[1+\alpha(\pi+1)]^2 + \alpha^2\pi^2\}^{1/2}[1+\alpha(\pi-1)]]\,. \quad (11)$$

This parameter is the half-width at half-maximum depth (HWHM) normalized by the Doppler width, ξ, which also corresponds to half the broadening of the line by Doppler motions. The line profiles and normalized half-widths given by equations (9)–(11) are shown in Figure 2b. Like the zeros of the Fourier transform, $\chi_{1/2}$ also depends on the limb darkening (see Table 2 and Fig. 2*b*), so that variations in the limb-darkening coefficient will be reflected as variations in the associated V sin i. Taking the range of values for $\chi_{1/2}$ for the full range of α, we see that $3^{1/2}/2 \geq \chi_{1/2}(\alpha) \geq 2^{1/2}/2$, which amounts to a range of about 26% about the reference value of $\chi_{1/2}(\alpha = 0.6)$. As was the case with the zeros of the Fourier transform, this argument relies on the line profile being characterized by a single value of the limb-darkening coefficient.

From the definition of the Doppler width given in equation (7), we may express the value of V sin i as

$$V \sin i = \Delta\lambda^f_{1/2}(c/2\lambda_0\,\chi_{1/2})\,. \quad (12)$$

Here we have replaced the "observed" value $\Delta\lambda$ with $\Delta\lambda^f_{1/2}$ (FWHM), which requires the factor of 2 in the denominator. Now we are prepared to compare the values of V sin i yielded by the CMRS with those that result from a rotating model where the spectral lines are the result of physical processes and have been calculated ab initio.

3. THE AB INITIO MODELS: COMPARISON WITH THE CMRS

All analysis of stellar line profiles relies on the comparison of observational profiles with those generated by theory. In order to verify the efficacy of the CMRS, we will use it as a basis for analyzing line profiles resulting from the models generated by Collins, Truax, & Cranmer (1991). This has the advantage that all the basic parameters of the modeled star are known in advance, and the observational noise can be taken to be zero. Thus, a direct test of the CMRS is possible. We shall examine the values of V sin i that result from the analysis of different lines for different model stars using both the zeros of the Fourier transforms and the line half-width to obtain those values. Since we have already discussed the effect of limb darkening on the results obtained from the CMRS, we will choose Carroll's (1928) value of $\alpha = 0.6$ for the "combined limb-darkening coefficient." We will then compare that value with the actual values appropriate for the continuum near the lines used for analysis.

Collins et al. (1991) calculated the line profiles for a number of spectral lines which occur in early-type stars. Models were made which rotated at various speeds and had various angles of inclination. From those models we shall select spectral types B1 and B9 to represent the range of early-type stars and the lines He I λ4026, He I $\lambda\lambda$4470, 4471, and Mg II λ4481 as typical of the types of lines used to determine V sin i for these stars (see Fig. 4). While we shall also look at the values of V sin i obtained from the Fourier transform of He I $\lambda\lambda$4470, 4471, the inherent asymmetry of that line blend (see Fig. 4) will defeat the application of the FWHM method. In Table 3 we give the values of V sin i obtained from the first two zeros of the Fourier transforms of the lines of these models along with the values that result from the FWHM given by Collins et al. (1991). The traditional value of the limb-darkening coefficient $\alpha = 0.6$ was used to obtain these values. In Figure 5*a* we display the results for both spectral types B1 based on the first two zeros of the Fourier transforms for the CMRS. Figure 5*b* shows similar results for the B9 model based on the half-width of Mg II λ4481, as well as the zeros of the Fourier transforms of the broadening functions of the CMRS. The solid straight line

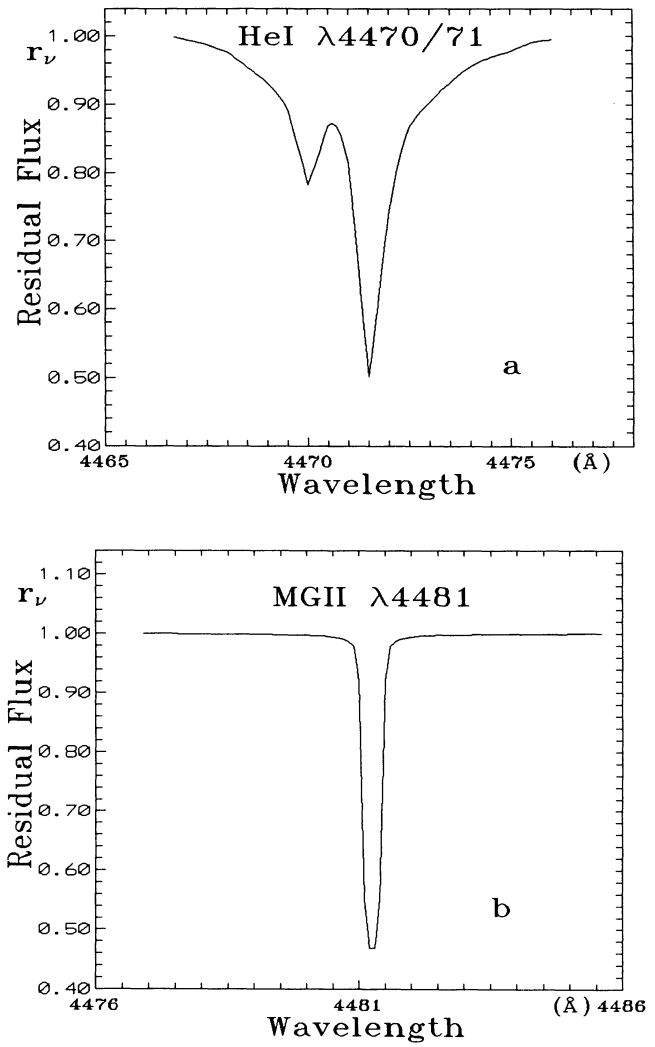

FIG. 4.—Line profiles used for the analysis of (*a*) the B1 V model (He I λλ4470, 4471) and (*b*) the B9 V model (Mg II λ4481). Since there is no rotational or instrumental broadening, the two components of He I λλ4470, 4471 are clearly visible. The thermal Doppler broadening and finite resolution used in the figure causes the two components of the Mg II λ4481 doublet to merge, forming the somewhat broadened base of the line.

is the "45° line" where all points would lie if the CMRS always yielded the correct results.

While there is no observational noise in the traditional sense for these models, the line profiles are calculated for a finite set of wavelengths within the line. This will result in sampling limits set by the Nyquist frequency limiting the range of the Fourier transforms that can be used for determining V sin i. This is the reason for the lack of values FT(x_1) in Table 3 obtained from the second zero of the Fourier transform for the line He I λ4026. In addition to the finite sampling errors, there is the usual problem of locating the continuum that plagues all observers. Our problem is not as difficult, for we do not have the observational noise present. However, the obvious solution of choosing a wavelength very remote from the line center will generally produce systematic differences with observational determinations. Such a procedure will fail completely for the He I λλ4470, 4471–Mg II λ4481 system that becomes blended at large rotational velocities. Here we have adopted the same procedures as Collins et al. (1991) for dealing with these problems.

The intrinsic line width will result in an overestimate of the value of V_e sin i for small values. This can be seen for the fractional velocity ($w = \omega/\omega_c$) of 0.5, and inclination $i = 30°$ models where the relatively intrinsically broad line of He I yields value of V sin i that are 10%–40% too large. The fact that the half-widths of Mg II λ4481 yield values of V sin i that are slightly smaller than the value of V_e sin i is due to the intrinsic sharpness of the magnesium line and an inappropriate treatment of the limb-darkening coefficient for the line (see § 4). The Fourier transform method is far less sensitive to the intrinsic width of the line. Thus zeros of the Fourier transform of the line are more closely associated with the shape of the rotationally broadened line, which is characteristically concave up. This is the reverse of the local mechanisms that intrinsically broaden the line. The strength of this aspect of the Fourier transform method is most clearly demonstrated by the results for He I λλ4470, 4471, which has an extremely complicated intrinsic line shape yet yields values of V sin i close to those of more reasonably shaped lines.

As is clear from the values in Table 1, the higher order zeros of the Fourier transform are less sensitive to the choice of the "combined limb-darkening coefficient," so we would expect them to yield a value of V sin i closer to V_e sin i than the lower order values. One can see for the values in Table 3 that this is indeed the case. However, in practice, this is usually offset by errors resulting from the sampling frequency. The extent to which the choice of the limb-darkening coefficient can affect the measured value of V sin i can be inferred from Figures 2*b* and 3*b*. While the values obtained for slow to moderate rotation fall within commonly accepted ranges of uncertainty for V sin i, the departures from the correct values for rapid rotation are well beyond those norms. The primary reason for the systematic departure of V sin i as determined from both the first and the second zero of the Fourier transform is the absence of gravity darkening in the CMRS. The gravity darkening effectively obscures the rapidly rotating equatorial regions of the star, yielding a line profile that is similar to that of a more slowly rotating star. Thus one expects the measured values V sin i to fall systematically below the true value of V_e sin i. For the He I λλ4470, 4471, the situation for the early B spectral types is made even worse by the dependence of the λ4470 "forbidden" component of the line on local gas pressure. The strength of that component is paradoxically increased at greater pressures due to the overlap of its wave function with the permitted transition of the λ4471 component of the line. Thus in the lower pressure environment that gravity darkening yields in the equatorial regions, He I λλ4470, 4471 will appear even weaker than one would expect from the corresponding drop in lowered flux. This effect is clearly shown in Figure 4*a*. Examples of the effects of rotation on the sharp lines shown in Figure 4 are shown in Figure 5 for the B1 V and B9 V models used in this study. The V_e sin i of the models and the V sin i corresponding to the half-widths of the lines shown in Figure 5 are given in Table 3.

In spite of its use in the determination of V sin i, the strength, intrinsic width, and blending of the He I λλ4470, 4471 might be considered an unfair test of the CMRS. To investigate this point, we considered the rotational effects on the simpler doublet Mg II λ4481. This line is also employed frequently in the determination of V sin i for the late B stars. Its symmetry also makes it an excellent candidate for the half-width method.

TABLE 3

V_e sin i OBTAINED FOR THREE SPECTRAL LINES OF THE B1 AND B9 ROTATING STELLAR MODELS

MODEL/i	MODEL V_e sin i	He I λ4026 FT(x_0)	He I λ4026 FT(x_1)	He I λ4026 $\Delta\lambda^f_{1/2}$	Mg II λ4481 FT(x_0)	Mg II λ4481 FT(x_1)	Mg II λ4481 $\Delta\lambda^f_{1/2}$	He I λλ4470, 4471 FT(x_0)	He I λλ4470, 4471 FT(x_1)
B1, w = 0.5:									
i = 30	85.2	88.5	...	125.4	86.0	84.3	83.5	86.4	91.0
i = 45	120.5	122.3	122.1	155.8	121.5	120.7	119.5	122.2	121.4
i = 60	147.7	143.8	152.2	180.7	150.2	145.5	147.8	140.6	153.5
i = 90	170.5	170.2	173.9	201.0	171.6	170.4	172.4	176.1	170.8
B1, w = 0.9:									
i = 30	179.0	178.2	177.1	205.1	180.1	180.0	185.6	182.3	175.0
i = 45	253.1	256.1	264.8	264.4	254.9	245.1	281.8	251.9	274.1
i = 60	310.0	292.7	308.1	303.5	332.1	297.8	363.9	285.6	302.7
i = 90	358.0	311.3	325.5	322.3	369.4	279.5	388.5	299.8	313.1
B1, w = 1.0:									
i = 30	245.4	233.1	239.6	243.1	236.6	235.2	249.4	231.1	262.8
i = 45	347.4	294.5	312.2	303.5	309.4	279.5	379.9	283.4	304.2
i = 60	425.4	309.0	327.2	317.2	420.9	297.8	378.5	302.3	317.8
i = 90	490.8	310.9	327.2	319.2	1206.6	244.2	387.6	307.4	322.6
B9, w = 0.5:									
i = 30	60.7	58.2	...	69.5	59.2	59.7	57.5	47.9	68.4
i = 45	85.8	76.4	...	88.3	83.8	84.2	84.4	76.5	88.2
i = 60	105.1	93.3	100.1	106.6	103.1	103.4	104.4	90.5	108.2
i = 90	121.4	107.8	111.2	120.3	119.1	119.8	122.2	111.6	115.1
B9, w = 0.9:									
i = 30	127.4	101.2	108.5	116.7	118.7	122.6	119.9	99.4	111.9
i = 45	180.2	138.9	152.4	155.8	236.6	244.2	174.7	137.4	158.5
i = 60	220.7	166.7	187.0	183.7	205.7	211.7	213.4	161.2	182.0
i = 90	254.9	189.9	212.7	201.5	236.6	244.2	246.7	177.8	199.0
B9, w = 1.0									
i = 30	174.8	115.8	123.7	134.5	142.0	148.5	147.3	116.3	122.8
i = 45	247.1	152.6	176.5	177.6	197.8	209.0	202.5	151.2	172.6
i = 60	302.7	184.5	202.4	202.5	233.5	250.9	244.4	181.4	185.1
i = 90	349.5	186.5	213.1	201.5	246.2	264.4	253.1	174.4	192.4

In addition to the results for the B1 V models, Table 3 contains results obtained for a sample of the rotating B9 star models of Collins et al. (1991) Since Mg II λ4481 shows behavior with temperature opposite to that of He I λλ4470, 4471, we might expect its increasing line strength to offset the effects of gravity darkening. However, as seen in Figure 6*b*, there is the same systematic departure of the measured value of V sin i at large rotational velocities for spectral type B9 V shown by He I λλ4470, 4471 for the B1 V model presented in Figure 6*a*. Therefore, the temperature dependence of Mg II λ4481 is insufficient to offset the effects of gravity darkening. Thus both methods show the same failing at large rotational velocities for Mg II λ4481 as was observed for the strong He I λλ4470, 4471 of the earlier spectral types. A similar failure was noted by Hardorp & Strittmatter (1968) for a somewhat different collection of He I lines where V sin i was determined by the half-width method. The uncertainty introduced by the choice of limb darkening is fairly symmetric for the Fourier transform method, but it is skewed strongly toward smaller values of V sin i for stars showing less limb darkening. This suggests that errors in the chosen values of the limb darkening will lead to values of V sin i which are systematically less than the correct value of V_e sin i. Certainly for intrinsically rapidly rotating stars, neither method will yield reliable results.

At small to moderate rotational velocities, both the Fourier transform and the half-width methods of determining V sin i yield values close to the actual value of V_e sin i. The range of values associated with each method is sufficiently large to cover the true values of V_e sin i easily. Indeed, it is remarkable that the reasonably arbitrary value for the "combined limb-darkening coefficient" of $\alpha = 0.6$ works as well for these stars as it does. While it is tempting to suggest that the near-gray structure of early-type stellar atmospheres makes the choice of the self-consistent value of the limb-darkening coefficient for the gray Eddington atmosphere (with the integrated Planck function as source function), $\alpha = 0.6$, appropriate for these lines, such is not the case. While the dominance of electron scattering in the opacity of B1 stars indeed makes them relatively gray, the behavior of the source function with frequency is unlikely to mimic the integrated Planck function except by chance.

However, before leaving this section, it is useful to determine the value of the continuum limb darkening appropriate for the part of the spectrum being investigated. To that end, the specific intensity and the cosine (i.e., μ) of the emergent angle were generated for the nonrotating models of spectral types B1 V and B9 V at $\lambda = 4475$ Å. These are shown in Figure 7. The long- and short-dashed lines represent linear least-squares fits to the solid curves determined from the ab initio models. In carrying out the least-squares fits, the specific intensity has been approximately weighted by the projected area of the stellar disk. The value of α for the He I line in the B1 star is a modest 0.37. However, the value of $\alpha = 0.57$ for the same wavelength at spectral type B9 V is, by chance, closer to the gray-atmosphere value used in the previous section. This larger value can be understood through the impact of the neutral hydrogen opacity on the Paschen continuum in the line-forming regions of the upper atmosphere of a B9 star. Temperatures in this region are more typical of the photosphere of an A2 star where the Balmer lines reach their maximum

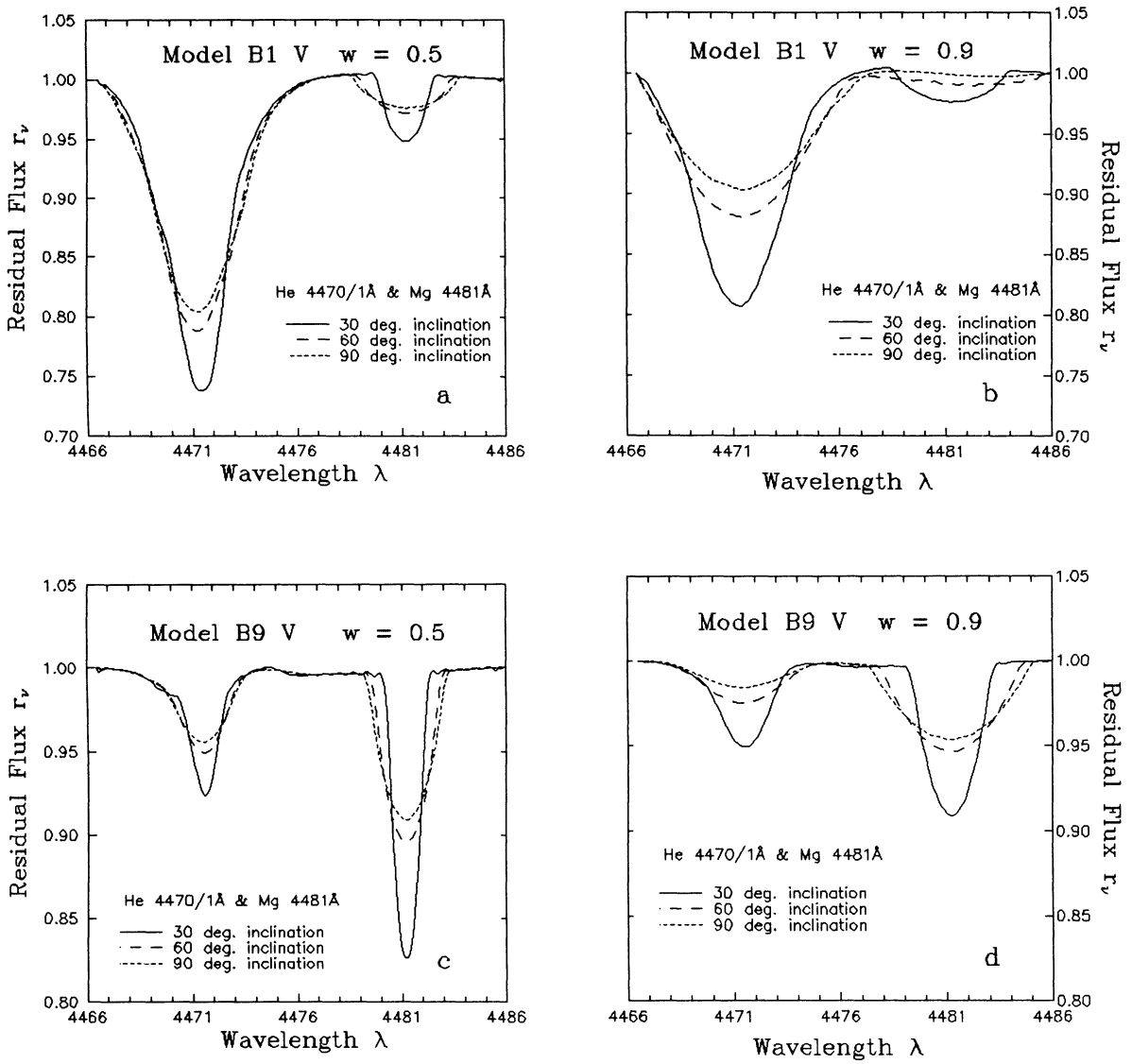

FIG. 5.—Examples of the line profiles from the ab initio models for spectral types B1 V and B9 V at fractional rotational velocities $w = 0.5$ and 0.9

strength and the neutral hydrogen absorption in the Paschen continuum will also be a maximum. This marked increase of opacity with height leads to a sharp increase in the temperature gradient with the resultant drop in the temperature of the upper regions of the atmosphere. The lower temperature yields a unusually low source function and thereby a rapid drop in the intensity as one approaches the limb. In addition, we have computed the values of the limb darkening appropriate for the center of each line used in the analysis. The behavior of the specific intensity at the line cores is shown at the bottom of each panel in Figure 7. The resulting values for the least-squares limb-darkening coefficients are given in Table 4 and are far less than the adjacent continuum values. This clearly demonstrates the failure of assumption 2 for the strongest part of the line which will dominate the resulting rotating line profile.

It is clear that the linear nature of the limb darkening can only be taken as a rough approximation. If one were to use the

TABLE 4

LIMB-DARKENING COEFFICIENTS FOR CONTINUUM AND LINES OF AB INITIO MODELS

Source		B1 V, $w = 0$, He I λ4471	B9 V, $w = 0$, Mg II λ4481
Continuum Values			
λ4475.00.....	α	0.37	0.57
	β	0.59	1.33
Line-Core Values			
λ4471.48.....	α	0.08	...
	β	0.09	...
Eq. (15).....	α	<0.14	...
	β	<0.16	...
λ4481.13.....	α	...	0.29
	β	...	0.41
Eq. (15).....	α	...	<0.32
	β	...	<0.47

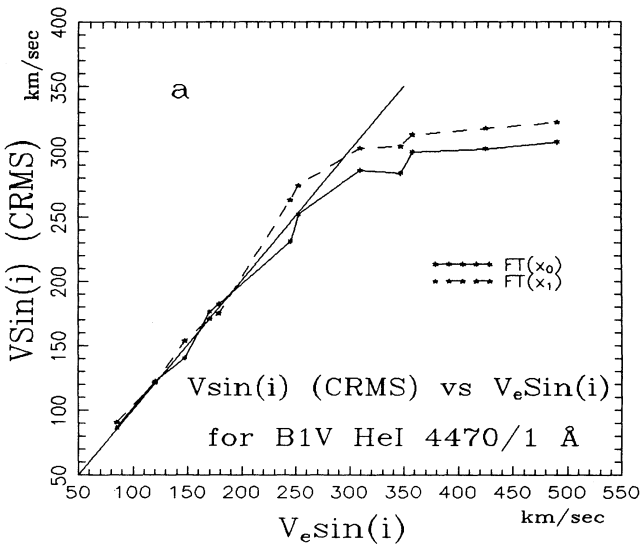

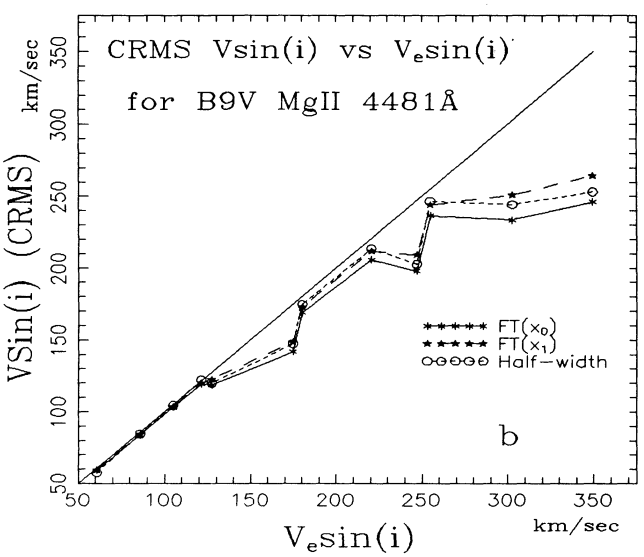

FIG. 6.—(*a*) Measured values for V sin i vs. V_e sin i for the B1 models of Collins et al. (1991) as determined from the first two zeros of the Fourier transform of He I λλ4470, 4471. The values have been calculated for the traditional value of limb darkening (i.e., $\alpha = 0.6$). The solid line denotes the results obtained from the first zero of the Fourier transform, while the dashed line corresponds to those derived from the second zero. (*b*) Values of V sin i determined from the first and second zeros of the Fourier transform (*solid line and long-dashed line, respectively*) of Mg II λ4481 as well as from the line's half-width (FWHM) (*short-dashed line*) vs. V_e sin i for the B9 stellar models of Collins et al. (1991). The irregularities appearing for moderately large V_e sin i result from combining various models with different inclinations and actually indicate the type of uncertainty one can expect by comparing the CMRS with ab initio models.

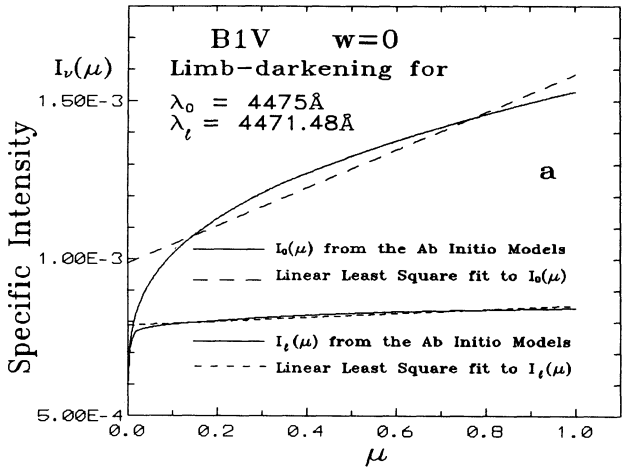

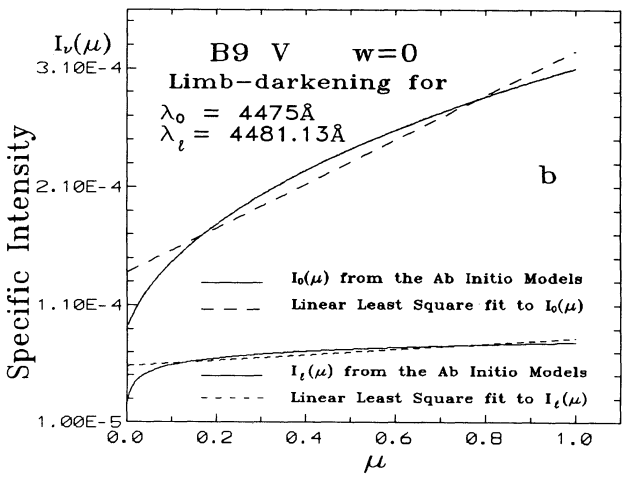

FIG. 7.—Dependence of the specific intensity at the continuum wavelength $\lambda = 4475$ Å and the line center λ_0 as solid lines with $\mu = \cos\theta$ for (*a*) the nonrotating B1 V and (*b*) the nonrotating B9 V models. The units may be regarded as arbitrary, since only ratios are involved in determining the limb-darkening coefficients. The long-dashed lines represent least-squares fits of the continuum specific intensity, where the values are approximately weighted by the local projected surface area. The resulting values of the limb-darkening coefficient α are given in the text and are $\alpha = 0.37$ and $\alpha = 0.57$ for the B1 V and B9 V models, respectively. The calculations for the continuum were made with the line opacity turned off, so that they truly represent a continuum. In the lower section of each panel $I_\nu(\mu)$ is shown for λ_l of the line core, and the least-squares fit is shown by the short-dashed line yielding values for the limb-darkening coefficient appropriate for the line cores of 0.08 and 0.29 for He I λ4471.48 in the B1 V model and Mg II λ4481.13 in the B9 V model, respectively (see Table 4).

extreme values of $I_\nu(\mu)$ (i.e., $\mu = 0, 1$) to obtain the value for the linear limb-darkening coefficient, values of α significantly larger than those described above which are appropriate for a flux-weighted mean would result. This is simply the result of the rapid nonlinear drop of the local temperature as one approaches the stellar surface and the corresponding drop in the specific intensity near the limb. Since a principal effect of rotational broadening is to map the contributions of certain parts of the stellar surface to specific regions of the resulting spectral line, these systematic departures from linearity can be expected to have systematic effects on the line profile itself. In the next section we will investigate the impact of these effects and limb-darkening values on the second assumption of CMRS, specifically the requirement that the value of the limb-darkening coefficient must be the same for the line and the continuum.

4. COMPARISON OF RESULTS FROM THE MCMRS WITH THE AB INITIO MODELS

In order to introduce a more physical description of the spectral line being investigated, a number of observers (e.g., Slettebak 1949; Gray 1976) have replaced the delta-function–like line of the CMRS with an empirically determined "sharp-

line" line profile for an appropriately equivalent-type star. This has the advantage of eliminating the theory required for the generation of the line, but introduces uncertainties of the comparison of the "sharp-lined star" and the target star of the investigations. It also assumes that an observed flux profile can replace the local specific intensity profile required by the model. Slettebak, Kuzma, & Collins (1980) have shown that rotation can introduce a change of one or more spectral subtypes over what would be expected for a nonrotating star of the same mass. Thus the appropriateness of the "sharp-line" profile, classically broadened, for comparison with a rotating star remains in doubt. The three assumptions of the CMRS given in § 1 are also assumed by the MCMRS. However, since the "sharp line" arises in a real stellar atmosphere, it is logical to inquire more closely as to the appropriateness of the linear limb-darkening law used for the continuum to describe the behavior of the line.

In § 3 we compared the ab initio models and the CMRS model by directly measuring the parameters associated with V sin i (i.e., the FWHM and the zeros of the Fourier transforms). In this section our comparison will be handled a little differently. We will try to follow the observer's procedure more closely. That is, we will take a "sharp-lined" star and broaden the appropriate line profile classically, and compare the result with the ab initio model having the same value of V_e sin i as the value of V sin i used to classically broaden the line. Again we will employ the full range of limb-darkening coefficients, $0 \leq \alpha \leq 1$, that was used earlier. We will concern ourselves largely with equator-on (i.e., $i = 90°$) and equatorial speeds appropriate for $w = 0.5$, 1 (see Table 3 for actual values). We have the distinct advantage here over the traditional observer that we have a sharp-lined star that is ideal for the comparison, namely, the nonrotating model (i.e., $w = 0$) which served as a basis for the ab initio models (see Figs 4*a* and 4*b*). In addition, we take advantage of knowing the correct answer and rotationally broaden the sharp lines to the correct value of V_e sin i. This is most easily done by multiplying the Fourier transform of the sharp line by the Fourier transform of the broadening function as found in equation (6). The amplitudes (i.e., Fourier moduli) of these Fourier transforms are shown in Figures 8 and 9 for spectral lines shown in Figure 4 for the models of B1 V and B9 V, respectively. The solid line above the three Fourier transforms covering the range in limb-darkening coefficients represents the Fourier transform of the appropriate line for the ab initio model itself. As would be expected from the analysis in § 3, the range of zeros nicely blankets the correct value for the zero of the Fourier transforms for moderate angular velocity (i.e., $w = 0.5$) for both spectral types, in spite of the fact that the asymmetrical line He I $\lambda\lambda$4470, 4471 was used for the determination for spectral type B1 V. However, the choice of limb-darkening coefficient should be quite different for the later type B9 than for the B1 models. A value of $\alpha > 0.6$ seems to be required for spectral type B9, while $\alpha \ll 0.6$ is more appropriate for the B1 models for a line only 10 Å to the blue of that used for the B9 comparison. These results are in qualitative agreement with the actual values for the continuum limb darkening obtained from the linear least-squares fits to the curves in Figure 7.

For the analysis of the line profiles themselves, the rotationally broadened half-width is affected by the choice of the sharp line profile. Thus, unlike the value of V sin i obtained by Fourier analysis, the value of V sin i obtained from the FWHM will depend on the choice of the local profile. Thus, we

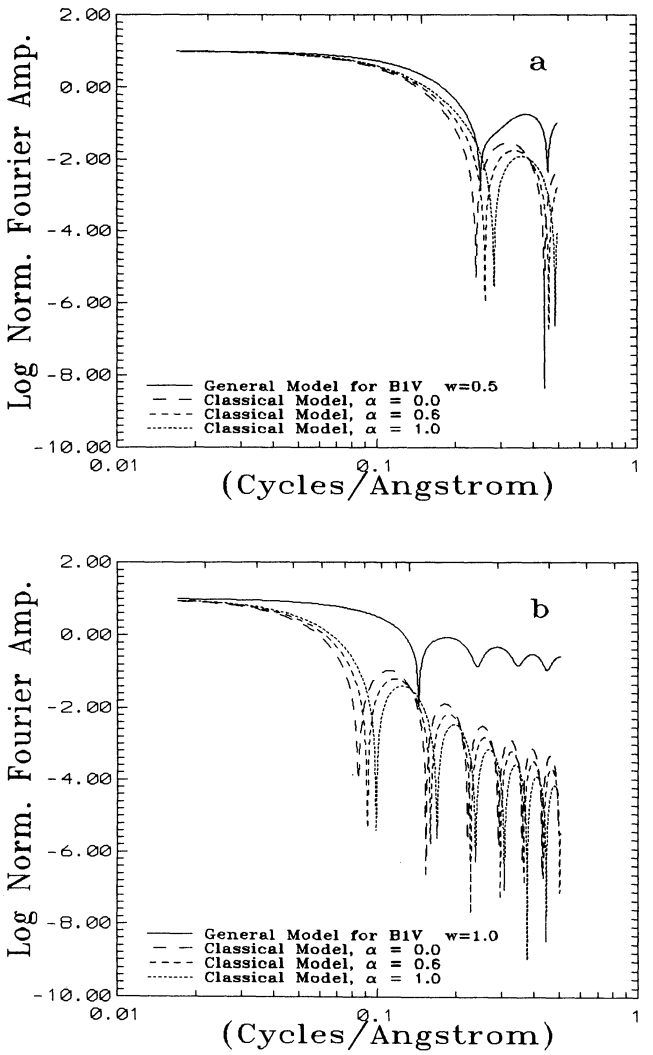

FIG. 8.—Fourier transforms of the classically rotationally broadened sharp line obtained from the nonrotating model compared with the rotating counterpart from the ab initio model. (*a*) Results for spectral type B1 V, $w = 0.5$; (*b*) results for a B1 V critical rotating model (i.e., $w = 1.0$). Results for the full range of limb-darkening coefficients are shown in both figures. All models are seen equator-on.

should expect a different level of accuracy here from that given in Table 3. However, for comparison with the Fourier analysis we have generated line profiles by convolving the sharp-line profile with the classical broadening function appropriate for the V_e sin i of the ab initio model for the full range of limb-darkening coefficients. For computational convenience, the convolution was accomplished by inverting the complex Fourier transforms used to prepare Figures 8 and 9. The results are displayed in Figures 10 and 11. As was the case for the CMRS, the FWHMs of the classically broadened line exceed those of the ab initio models for the same V_e sin i. However, in § 3 the comparison was made by equating the FWHM of the two which resulted in a lower V sin i for the CMRS. The reduction in the strength of the line He I $\lambda\lambda$4470, 4471 line discussed in § 3 is readily apparent in Figure 10*b*. This is expected because of the additional effects of extreme rotation affecting the line. However, for the modest rotation of $w = 0.5$ and $i = 90°$, the classical profiles are much closer to

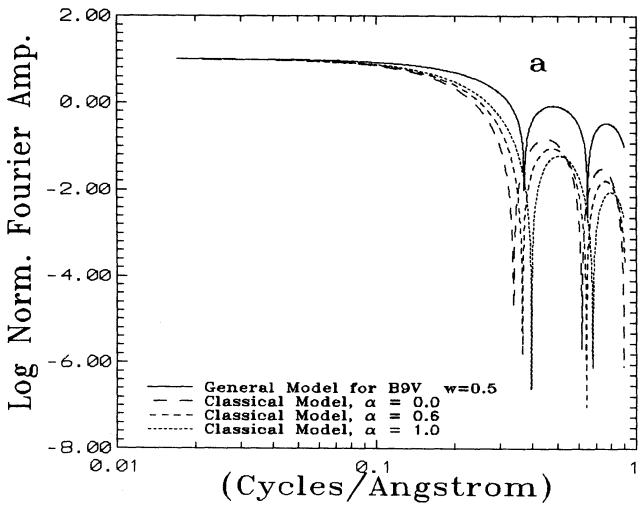

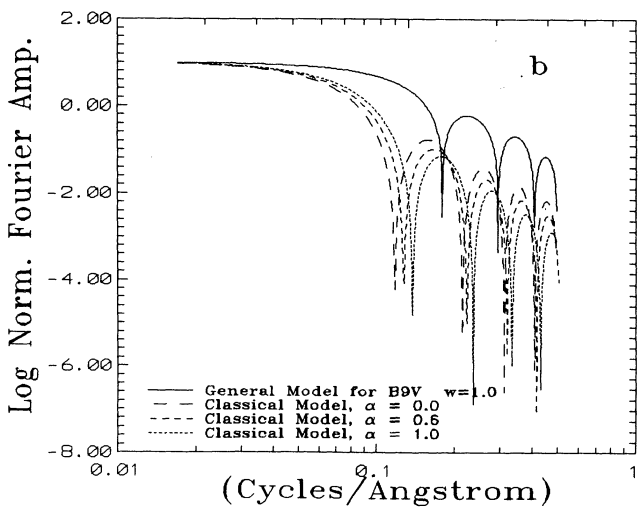

FIG. 9.—Same as Fig. 8, but for spectral type B9 V models

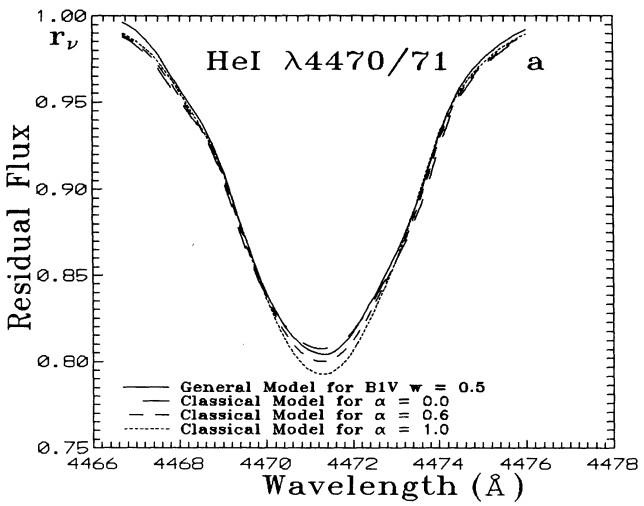

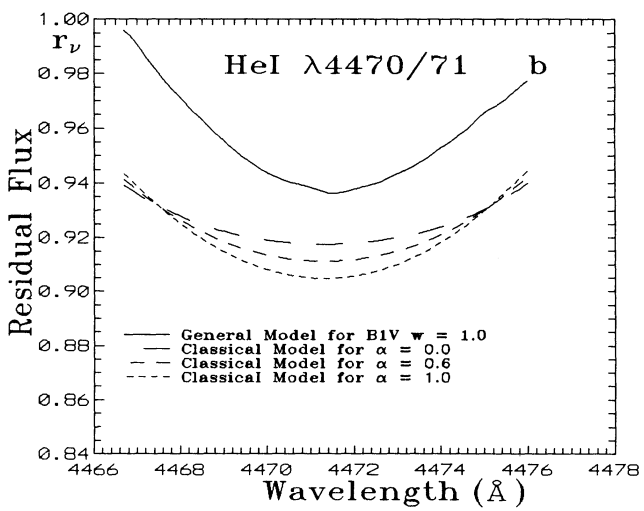

FIG. 10.—Sharp-line profiles of the nonrotating ab initio model with lines classically broadened for the full range of limb-darkening coefficients. These are compared with the rotating profile of the ab initio model having the same value of $V_e \sin i$. (*a*) Results for the moderately rotating B1 V, $w = 0.5$, model; (*b*) results for the critically rotating B1 V model. All models are seen equator-on. The considerable difference between the classically broadened lines and those of the critical rotator (i.e., $w = 1$) result from changes in the equivalent width of the critical rotator caused by the reduction in the local gravity.

those of the ab initio models. Here the rotation is large enough to remove most of the line asymmetry generated by the "forbidden" component of the line, but not so large as to involve the effects shown in Figure 10*b*. The limb darkening appropriate for the line seems to lie between 0 and 0.6 with a value of $\alpha \sim 0.3$ being quite plausible. However, Figure 11*a* indicates that a value of $\alpha \sim 0.9$, which is rather larger than the continuum value suggested by what would be more appropriate for the core of Mg II λ4481.

We may investigate this difference by examining the behavior of pure absorption lines with μ. By analogy with equation (1) we can write the behavior of the specific intensity in the line as

$$I_\nu(\mu) = I_\nu(1)[1 - \alpha_l(1 - \mu)] , \tag{13}$$

where α_l is the limb-darkening coefficient appropriate for the line and may be expected to vary within the line. However, since absorption lines require a temperature gradient for their production, they may be expected to vanish at the photospheric limb, so that the line intensity is the same as the continuum intensity. This suggests two conditions on the behavior of the intensity within the spectral line, which are

$$I_\nu(0) = I_c(0) ,$$
$$I_\nu(1) = I_c(1) f_\nu(1) , \tag{14}$$

where $I_\nu(1)$ is the residual intensity of the line for $\mu = 1$ at the center of the disk. Here $f_\nu(\mu)$ is the residual (i.e., normalized) specific intensity profile of the line. Thus, $f_\nu(1)$ is the residual specific intensity profile appropriate for the center of the disk. Combining this with equation (1), we arrive at an expression for the difference between the limb-darkening coefficient appropriate for the line and that of the continuum:

$$\delta\alpha \equiv \alpha_c - \alpha_l = [1 - f_\nu(1)](1 - \alpha_c)/f_\nu(1) > (1 - r_\nu)(1 - \alpha_c)/r_\nu . \tag{15}$$

Here we find results similar to those arrived at in § 2. Here r_ν is

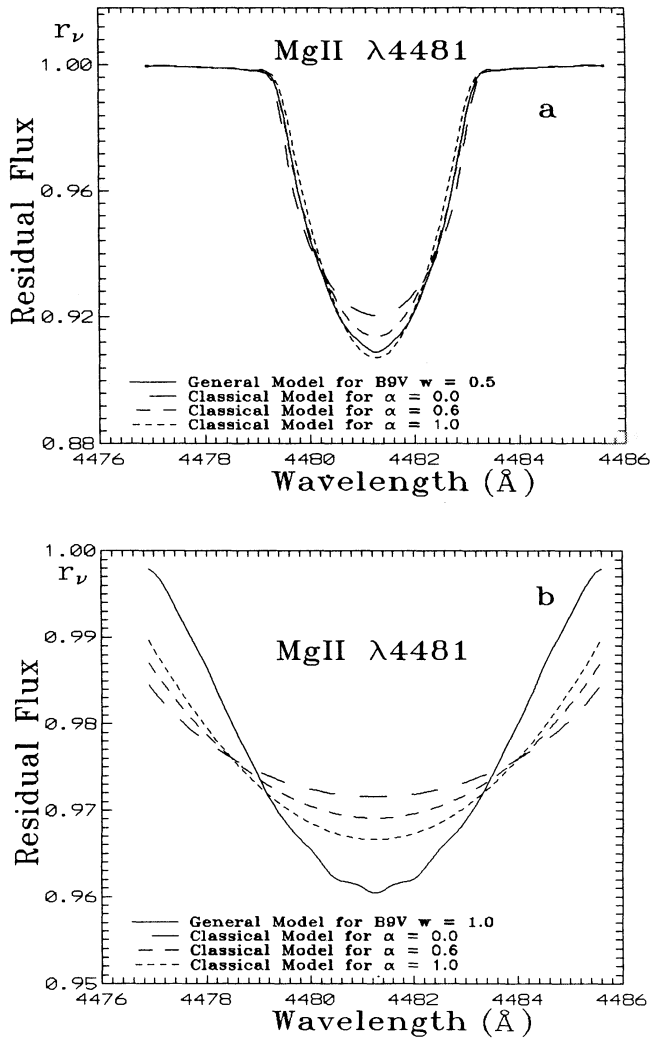

FIG. 11.—Same as Fig. 10, but for spectral type B9 V and Mg II λ4481

the residual flux in the line, which is generally less than the residual specific intensity at the center of the disk, $f_\nu(1)$. A steep source function gradient implies large limb darkening, so that $\delta\alpha(\nu) \approx 0$ so long as the line is not too strong (i.e., $f_\nu > 0$) and assumption 2 will be justified. However, equation (15) allows us to estimate quantitatively the extent to which this assumption is satisfied for any specific case. The right-hand side of equation (15) contains the residual flux for the specific line which must be measured in order for the line to be used. Thus we may place a lower limit on the magnitude of $\delta\alpha$ for any specific case. If we apply it to our lines and take r_ν from Figure 7, we find for He I λλ4470, 4471 a value of $\alpha_l = 0.14$ is appropriate for the line core, which is considerably less than the value obtained by fitting the moderately rotating lines in Figure 10*a*. The situation for Mg II λ4481 at spectral type B9 yields a value of $\alpha_l = 0.32$ for the line core. To obtain these estimates for the limb darkening in the line cores, we have determined α_c in equation (15) by approximating $I_\nu(\mu)$ with straight-line fits between $\mu = 0$ and $\mu = 1$. Had we used the area-weighted values obtained by the least-squares lines from Figure 7, we would have obtained the even lower values mentioned earlier and given in Table 4. We may verify the efficacy of this procedure by comparing the estimated values for the limb darkening of the line cores with their area-weighted values, which are summarized in Table 4. As expected, the values estimated from equation (15) exceed the area-weighted values. As noted earlier, the comparison of the least-squares values for both the line and the continuum suggest that assumption 2 fails badly for these lines so commonly used for the determination of $V \sin i$. This result is reinforced by noting that it is the line core that is most instrumental in determining the shape of rotationally broadened spectral lines.

Thus, the effects of limb darkening on the MCMRS are much the same as for the CMRS as shown in Figure 3*a*. The analysis of these two lines seems to suggest that a value of the limb darkening appropriate for the continuum yields results as close as can be expected to the correct values. However, it would be rather optimistic to conclude that this is a general result which can be applied to other lines for other spectral types. It must be remembered that the limb darkening in the line is a strong function of frequency and that the actual behavior often departs from being linear (see Fig. 7). This implies that there are limitations to the MCMRS even in the case of slow rotation.

Normally one does not worry too much about the departures from linearity of the law of limb darkening in analysis where the entire disk of the star is concerned (e.g., in the analysis of eclipsing binary stars), since the failure in linearity occurs largely near the limb, where the darkening itself has reduced the contribution to the integrated light. However, as Collins & Cranmer (1991) pointed out, Doppler broadening of spectral lines breaks the symmetry about the line of sight, since different parts of the disk contribute preferentially to different parts of the rotationally broadened line profile. Thus the properties of the limb will dominate the contribution to the wings of the rotationally broadened line. While the effect will influence all parts of the line, the wings of the line will be affected the most. Thus the departures from linearity will have the greatest influence on the Fourier transform whose low-order zeros are most influenced by large-scale systematic features in the line profile. Conversely, the effect on the half-width should be less, since the contributions in the vicinity of the half-Doppler width originate primarily well away from the limb of the star. Finally, since the rotational symmetry breaking increases with $V_e \sin i$, we would expect the nonlinearity of the limb darkening to become more of a problem with large velocities. However, in the regime of large velocities so many failures of the assumptions of the CMRS become apparent that it is difficult to specify which is dominant.

5. MEASUREMENT OF HIGHER ORDER PROPERTIES OF THE STELLAR VELOCITY FIELD

A number of authors have taken the departures of observed line profiles and their Fourier transforms from their classical counterparts to infer additional components of the photospheric velocity field. Stoeckley (1968a, b, c) and Stoeckley & Buscombe (1987 and references therein) used departures of observed line profiles from their classical counterparts to separate V_e from sin i as well as determine the extent of differential rotation and macroturbulence present in the atmospheres of stars. Gray (1977, 1981a, b, 1982) used the departure of the spectral line Fourier transforms from the classical transforms to determine the extent of differential rotation and macroturbulence in various stars. In this section we consider the extent to which the actual velocity field of the star can be determined by the information contained within the entire line

profile or its Fourier transform. The ab initio models used in this study have no motion present other than the macroscopic uniform rotational motion superposed on the thermal Doppler motion of the hot photospheric gases. There is no macroturbulent velocity included in the profiles. The typical numerical accuracy of the line profiles is of the order of 0.1%, and the computational accuracy of the classical broadening procedure is such as to not significantly degrade that accuracy. The choice of the continuum can be made in a consistent manner which any observer would envy. In addition, our "observations" are not plagued with instrumental broadening or noise. Thus we suggest that differences that occur between the CMRS and MCMRS and the ab initio models result from a failure of the classical assumptions of the CMRS and MCMRS to be realized in the more physical ab initio models.

Figures 8–11 show that attributing such differences to other motions is risky at best. It would seem reasonable to assume that these differences would also be found in the analysis of real stars. What is somewhat surprising is that failure occurs not only for extreme rotation ($w = 1.0$), as is expected, but also for the more moderate speeds described by the $w = 0.5$ models. Indeed, as can be seen in Figure 9*a*, the poor match between the Fourier transforms of the classically broadened sharp-line profiles and those of the ab initio models is present for even the fairly classical line Mg II λ4481 at moderate rotation. The Fourier transforms of the classically broadened sharp lines seem to fall consistently below those of the ab initio models. The reduced power at higher frequencies suggests that the rotational profiles of the ab initio models are more complex than those of the classically broadened models and require a greater contribution from the higher frequencies than their classical counterparts. If one considers all of the possible contributions to that complexity accounted for in the ab initio models for rapid rotation, that result is not to surprising. It is surprising that there are problems with the slower values of rotation for such a well-behaved line as Mg II λ4481. One possible explanation for the departure may be found in the doublet nature of Mg II λ4481. Although the infinite resolution used for the display and the turbulent thermal broadening conceal the doublet nature of the line in Figure 4*b*, it is included in the calculations of the ab initio models. Earlier studies showed that its inclusion was necessary to calculate correctly the equivalent widths of the line. It is possible that its doublet nature may affect the shape of the resulting line in a subtle manner leading to the differences shown in Figure 9*a*. While these may seem small, it should be remembered that the macroturbulence expected in these stars is a very small fraction of the rotational velocity of the typical B star.

The situation for the analysis of the line profiles themselves is fraught with equal difficulties, as can be seen from Figures 10 and 11. The departure of the line profiles from their classical counterparts is more subtle than that of the Fourier transforms. This can be traced to the different influence that higher frequencies have on the shape of the Fourier transforms as compared with the line profiles themselves. Thus we may expect difficulties in determining the extent of macroturbulence from the line profiles themselves similar to those encountered in analysis of the Fourier transforms. At large rotational velocities such as those shown in Figures 10*b* and 11*b*, even the half-width does not supply useful estimates of V_e sin i. Indeed, as Collins & Smith (1985) observed for the A stars, the line profiles for extreme rotation are not even unique with respect to inclination. Thus, the hope of determining other properties of the atmospheric velocity field from departures of the classical rotationally broadened profile from that of an actual star would appear to be elusive at best.

Finally, we consider the influence of intrinsic rotation at low inclination on the properties of the sharp line. There is no independent way that an observer can be assured that the sharp-lined star chosen for the reference star in any analysis is indeed an intrinsically slowly rotating star. In some instances the lines of a pole-on rapid rotator can be quite different from those expected for a nonrotating star of the same mass. While Collins (1987) has shown that this effect can be quite large for the Balmer lines, and Slettebak et al. (1980) found similar problems for He I $\lambda\lambda$4470, 4471 and Mg II λ4481, the effect on the Fourier transforms has never been investigated. In Figure 12 we show what is probably the worst case where the Fourier transforms of the He I $\lambda\lambda$4470, 4471 line profiles for a pole-on extreme rotator and a nonrotator are compared. We have ignored the first two zeros, since absolutely no differences are present until one gets to the higher order zeros of the Fourier transform. Even here the values of the zeros are unaffected. Only the amplitudes are very slightly modified. Thus one may conclude that concern about hidden intrinsic rotation of the sharp-lined star is not a fundamental concern for the determination of V sin i.

6. SUMMARY AND CONCLUSIONS

In this paper we have reviewed the development of the classical model of a rotating star (CMRS) developed by Carroll, Struve, Unsöld, and others, and its implications for the determination of the rotational velocities of stars. Although the simplifying assumptions on which the classical models rest lead to rotational profiles that are easy to interpret, they also introduce systematic errors that limit their utility. It has been known for some time (see Slettebak et al. 1975) that line profiles of the most rapidly rotating stars do not have half-widths that are uniquely related to V sin i. This can be seen by noticing the very flat nature of the curves in both Figure 10*b*

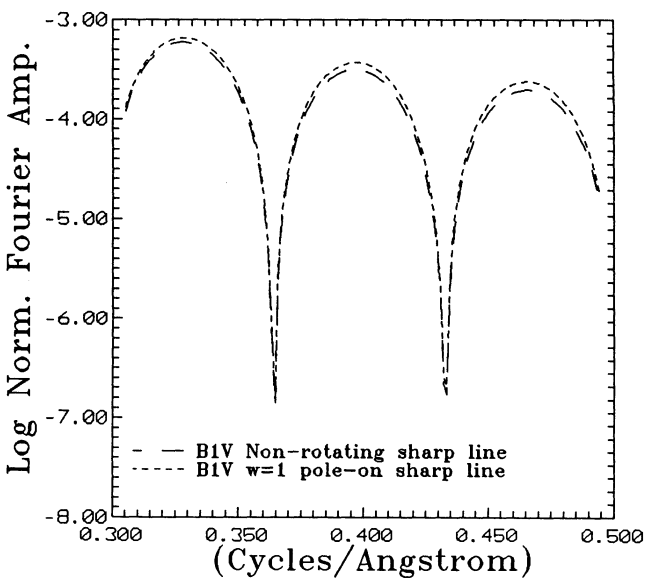

FIG. 12.—Fourier transforms for the higher order zeros (i.e., $x_{3,4}$) of the He I $\lambda\lambda$4470, 4471 line displayed in Fig. 7*a* and that of a pole-on rapid rotator. The marked similarity suggests that hidden extreme rotation should not be a great problem when picking a sharp-lined star.

and Figure 11*b* or by scanning the values in Table 3 for the most rapidly rotating models. This largely arises from the failure of all three assumptions of the classical models so that errors in the determination of $V_e \sin i$ of 50% or more may occur. Thus, for stars that rotate with angular velocities about 90% of their critical velocities or larger, the common methods employing the half-width or the popular Fourier transform of the line profile yield values of the rotational velocity that are systematically too low. The magnitude of the error can approach 50% of the true value for stars rotating at their critical velocity viewed equator-on. Errors of this magnitude confirm the suggestion by Collins (1970) that line profiles alone provide a poor method for the detection of the most rapidly rotating stars. The systematic nature of these departures from the correct value have serious implications for statistical studies of the rotational velocities of stars. However, systems such as those developed by Slettebak et al. (1980) and Slettebak, Collins, & Truax (1992) avoid much of the problem by directly comparing the observed line profiles with those of essentially ab initio models having known rotational velocity and inclination. Even these systems recognize the imprecision with which the rapidly rotating stars can be measured, by placing very large uncertainties on their values.

It is unlikely that this problem can be removed by including analyses of other spectral lines. The similarity of the departures for the very different strong lines of Mg II λ4481 and He I $\lambda\lambda$4470, 4471, which agree with the results of Hardorp & Strittmatter (1968), assures this. The situation is further confirmed by the purely practical matter that there are very few lines present in the spectra of these stars. Absence of the large photometric effects expected for the extreme rotating stars has led Collins & Sonneborn (1977) to suggest that it is likely that very few stars rotate faster than 90% of their critical velocity. However, it is clear from the values in Table 3 that, even at 90% of critical velocity, departures as large as 40% of the actual value of $V_e \sin i$ may result from employing the classical model. This is of particular significance for the study of Be stars.

However, it was felt that slow to moderate rotating stars could be well approximated by the MCMRS if not by the CMRS itself. Unfortunately, the development in § 3 suggests that even here assumptions 2 and 3 fail by introducing systematic errors. Should the limb darkening be moderate or low, then the limb darkening appropriate for the spectral line is likely to differ significantly from that of the continuum if the line is strong enough to provide reliable profiles for measurement of $V \sin i$. Since the instrumental broadening becomes more important at smaller values of $V \sin i$, prudence would suggest that no value of $V \sin i$ be considered to represent $V_e \sin i$ to better that 10% except in exceptional cases.

While there are special cases where the continuum limb darkening is quite large, such as the blue part of the spectrum of K and M stars, it should be remembered that the weak wavelength dependence of H^- throughout the late A, F, and G spectral types leads to limb-darkening coefficients similar to those of the Sun. Thus assumptions 2 and 3 of the MCMRS will fail for these stars as well. Again prudence would dictate caution in interpreting the meaning of $V \sin i$ at precision better than 10%.

For the early-type stars in general, the lines used for studying rotation are strong lines. The cores of such lines are usually saturated, implying that they are formed high up in the stellar atmosphere at all points on the apparent disk. This suggests that the intensity of the line core will not vary significantly across the apparent disk of the star, so that the limb darkening of the line core will be very small (see Fig. 7). Thus assumption 2 will be violated for virtually all early-type stars. The validity of the estimates of equation (15) are confirmed by direct calculation for the line cores shown in Figure 7. This strengthens the application of equation (15) to stars outside the realm of this study. While equation (15) suggests that the larger values of the continuum limb darkening may improve the situation for the late-type stars, a closer inspection shows that $\delta\alpha_c \sim (1 - \alpha_c)/f_v$ as $\alpha_c \rightarrow 1$. However, since the line core will tend to preserve the intensity of the limb, f_v will be small approaching zero, leaving the result of equation (15) indeterminate. The relevant point to remember is that most lines in late-type stars have exceedingly dark line cores, meaning that these lines will have core limb-darkening coefficients much less than the value appropriate for the continuum. Thus assumption 2 is suspect even for the late-type stars.

It must be remembered that the effective limb-darkening coefficient of the line will vary throughout the line from the continuum value in the wings of the line to a reduced value in the line core. Since the line core provides most of the absorption in the rotationally broadened line, its value will be dominant in determining the shape of the line, but the variability of the line limb-darkening coefficient will ensure that its shape departs from that of the MCMRS for any single value of the limb darkening. Further differences between rotationally broadened stellar lines and the classical models will result for the departures of the limb darkening from the simple linear relation required by the CMRS and the MCMRS. Thus differences between the line profiles of the MCMRS and the simple ab initio models used in this study arise from the failure of the MCMRS itself and cannot be interpreted as resulting from additional atmospheric motions.

However, the uncertainties in rotationally broadened line profiles are not limited to the problems of comparison with the theoretical models discussed in §§ 4 and 5. There are likely to be additional aspects to the photospheric velocity field of the star itself. The atmospheric velocity fields of real stars probably do include macroturbulence and perhaps differential rotation in their photospheric velocity fields. Cranmer & Collins (1993) make a persuasive case for the presence of large-scale zonal flows exhibiting speeds of the order of the macroscopic rotational velocity in these stars. It is clear that the presence of such flows would greatly complicate the analysis of rotationally broadened line profiles.

Finally, there is an elegant and fairly simple mathematical argument that emphasizes the futility of such an approach. Since a general stellar velocity field is at least a two-dimensional, if not three-dimensional, vector field, the information required to specify it would have the same cardinality (i.e., $\aleph_2$) as the functions which cover the Euclidean plane. However, the cardinality of the number of points in a single one-dimensional line profile is $\aleph_1$. Thus there is simply not enough information in a single spectral line to accomplish the unique specification of the general atmospheric velocity field. Even in the case where one uses a countable number of spectral lines, we are limited by $\aleph_0 \aleph_1 < \aleph_2$. Thus it would appear that even in principle the determination of a general velocity field from the analysis of stellar line profiles is doomed to failure. One might argue that forcing a model of the velocity field on the star reduces the number of possibilities sufficiently for a determination to be possible. Indeed, it is such an analysis that allows the determination of $V \sin i$ in the first place. That is, it is assumed that the macroscopic rotational velocity is so large

as to dominate all other aspects of the atmospheric velocity field as seen by the observer. For the early-type stars this is a good assumption. Thus one may use the CMRS to determine $V \sin i$ for a star as long as one does not expect accuracies greater than 10% under ideal conditions, with significantly larger errors for stars exhibiting extreme rotation. However, investigations which use the CMRS or the MCMRS to pursue additional aspects of the velocity field of the stellar atmosphere can be expected to yield results plagued with systematic error.

One of the authors (G. W. C. II) would like to extend his thanks to Paul Mason for his aid in transferring essential programs from the computers at the Ohio State University to those of Case Western Reserve University and in carrying out some of the calculations required for the continuum and line core limb darkening of the ab initio models. Additional thanks are due the anonymous referee whose careful reading and most professional response allowed a significant improvement in the presentation of our material.

REFERENCES

Carroll, J. A. 1928, MNRAS, 88, 548
———. 1933, MNRAS, 478
Carroll, J. A., & Ingram, L. J. 1933, MNRAS, 93, 508
Collins, G. W., II. 1970, in Stellar Rotation, ed. A. Slettebak (Dordrecht: Reidel), 85
———. 1987, in The Physics of Be Stars, ed. A. Slettebak & T. P. Snow (Cambridge: Cambridge Univ. Press), 3
———. 1989, Fundamentals of Stellar Astrophysics (New York: Freeman)
Collins, G. W., II, & Cranmer, S. R. 1991, MNRAS, 53, 167
Collins, G. W., II, & Smith, R. C. 1985, MNRAS, 213, 519
Collins, G. W., II, & Sonneborn, G. H. 1977, ApJS, 34, 41
Collins, G. W., II, Truax, R. J., & Cranmer, S. R. 1991, ApJS, 77, 541
Cranmer, S. R., & Collins, G. W., II. 1933, ApJ, 412, 720
Gray, D. F. 1976, The Observation and Analysis of Stellar Photospheres (New York: Wiley)
———. 1977, ApJ, 211, 198
———. 1981a, ApJ, 251, 152
———. 1981b, ApJ, 251, 155
———. 1982, ApJ, 258, 201
Gray, D. F. 1988, Lectures on Spectral-Line Analysis: F, G, and K Stars (Aylmer: Aylmer Express Ltd.)
Hardorp, J., & Strittmatter, P. A. 1968, ApJ, 153, 465
Shajn, G., & Struve, O. 1929, MNRAS, 89, 222
Shapley, H., & Nicholsen, S. B. 1919, Comm. Nat. Res. Sci. Mt. Wilson Obs., Vol. 2
Slettebak, A. 1949, ApJ, 110, 498
Slettebak, A., Collins, G. W., II, Boyce, P. B., White, N. M., & Parkinson, T. D. 1975, ApJS, 29, 137
Slettebak, A., Collins, G. W., II, & Truax, R. J. 1992, ApJS, 81, 335
Slettebak, A., Kuzma, T. J., & Collins, G. W., II. 1980, ApJ, 242, 171
Stoeckley, T. R. 1968a, MNRAS, 140, 121
———. 1968b, MNRAS, 140, 141
———. 1968c, MNRAS, 140, 149
Stoeckley, T. R., & Buscombe, W. 1987, MNRAS, 227, 801
Unsöld, A. 1955, Physik der Sternatmosphären (2d ed.; Berlin: Springer-Verlag)
von Zeipel, H. 1924, MNRAS, 84, 655